

Plasma Jet Printing: An Introduction

Jacob Manzi[®], Nirmala Kandadai, *Senior Member, IEEE*, Ram P. Gandhiraman[®], and Harish Subbaraman, *Senior Member, IEEE*

Abstract—Plasma jet printing is an emerging alternative to popular 2-D printing techniques, such as inkjet and aerosol jet printing. The inherent nature of the plasma provides films with good adhesion upon printing without the need for thermal sintering. The reduced logistics and the ability to print a wide range of materials on rigid and flexible substrates make it a valuable technique for printed and flexible electronics. In this tutorial article, we discuss the principles behind plasma printing, printer hardware, and printing mechanisms and provide representative print results.

Index Terms—Flexible electronics, Internet of Things (IoT), microplasma, plasma jet, printed electronics, selfsintering.

I. INTRODUCTION

THE rapid emerging of the Internet of Things (IoT) has created a huge demand for flexible and printed electronics (FPE) devices ranging from sensors, antennas, radio-frequency identification (RFID) tags, batteries and supercapacitors for energy storage, electrodes and displays to thin-film transistors, circuits, memory, and capacitors [1], [2], [3], [4], [5], [6], [7], [8], [9], [10], [11], [12]. Wearable devices for healthcare monitoring constitute another major application [13], [14], [15]. A wide variety of flexible and stretchable substrates, such as polymers, paper, textile and thin metal foils, support the above devices produced through rapid and inexpensive techniques in contrast to the clean room-based microfabrication technology. Jetting-based printing methods, such as inkjet printing (IJP) and aerosol jet printed AJP, have been widely used to print the devices in the above applications [1], [2], [3], [4], [5], [6], [7], [8], [9], [10], [11], [12], [15], [16], [17], [18], [19]. Besides low cost and reduced logistics relative to most past technologies, the advantages include feature resolution of 10 µm achievable at

Manuscript received 29 November 2022; revised 14 February 2023; accepted 21 February 2023. Date of publication 13 March 2023; date of current version 24 March 2023. The work of Ram P. Gandhiraman was supported by the NASA Small Business Innovative Research (SBIR) Award under Contract 80NSSC19C0136. The work of Harish Subbaraman was supported in part by the NASA Established Program to Stimulate Competitive Research (EPSCoR) under Project 80NSSC19M0151 and in part by the NSF under Award CMMI-1825502. The review of this article was arranged by Editor P. Thadesar. (Corresponding authors: Ram P. Gandhiraman; Harish Subbaraman.)

Jacob Manzi, Nirmala Kandadai, and Harish Subbaraman are with the School of Electrical Engineering and Computer Science, Oregon State University, Corvallis, OR 97331 USA (e-mail: harish.subbaraman@oregonstate.edu).

Ram P. Gandhiraman is with Space Foundry Inc., San Jose, CA 95133 USA (e-mail: ram@spacefoundry.us).

Color versions of one or more figures in this article are available at https://doi.org/10.1109/TED.2023.3248526.

Digital Object Identifier 10.1109/TED.2023.3248526

present, elimination of photolithography, minimized contamination due to the noncontact nature, rapid prototyping, good biocompatibility with many substrates, large area printing, and the ability to print a wide a range of metals, semiconductors, and dielectrics.

In addition to meet the demands of the above emerging applications, printing has the potential to support the back end of line (BEOL) needs of the silicon IC industry [20]. Copper pillars aim to replace the conventional lead-eutectic solders due to health concerns of lead, low conductivity, and dimensional limitations. Electroplating is used to create copper pillars with the aid of masking, which results in wasted chemicals. Conductive epoxy resins are also explored. Through silicon vias (TSVs) are used when ICs are stacked-up vertically as vertical interconnect providing contact between various layers of the die, which is simply a trench created by reactive ion etching (RIE) and filled with metal. As these are pressing problems, the IC industry and research community are very active in seeking solutions, including new materials and approaches to achieve the above functions while keeping high reliability. In that regard, additive techniques are being explored to create copper pillars and TSV filling instead of the conventional subtractive processes, such as RIE. For example, IJP is capable of creating vertical metal structures with thickness exceeding lateral dimensions in a layer-bylayer approach. Current capabilities allow printing structures with base dimensions of 20–50 μ m and aspect ratios ~100, as demonstrated in [21] and [22]. Thus, the printing technologies, besides spurring new applications of flexible and wearable devices, are poised to provide aid to established industries, such as IC manufacturing.

There are several practical issues with IJP and AJP in the above applications. The foremost is that "printing" does not give a thin film ready for device fabrication; rather, it just delivers the ink particles to the substrate resulting in unconnected or poorly connected nanoparticles (NPs) with poor film quality (for example, very high resistance). Therefore, a thermal treatment afterward is always needed to get desirable film morphology with curing or annealing temperatures of 100 °C-400 °C, lasting few minutes to few hours. The high-temperature sintering eliminates selection of delicate substrates, such as paper and fabric, from consideration in certain applications. Alternative low temperature and rapid sintering approaches, such as laser, photonic, chemical, and plasma sintering, have been advocated and demonstrated [23], [24], [25] with varying degrees of success. Additionally, a surface pretreatment may be needed in some cases, depending on the combination of the substrate and target material to be printed. Thus, printing indeed becomes a three-

0018-9383 © 2023 IEEE. Personal use is permitted, but republication/redistribution requires IEEE permission. See https://www.ieee.org/publications/rights/index.html for more information.

step process (pretreatment and posttreatment and printing) requiring three pieces of equipment, resulting in additional operating costs and process times, increased logistics, and floor space. The thermal sintering step could result in pinholes and other defects including inevitable oxide layer formation during the endless number of print-cure cycles often used for building the desired film thickness. This becomes an even bigger issue when dealing with complex nonplanar 3-D objects as baseline substrates. Removing the binders or solvent is often problematic especially when multilayers of materials need to be printed. Tuning the material properties, such as oxidation state, dielectric constant, polymerization, and so on, is challenging with these techniques. Finally, the dependency on capping agents and organic solvents in the metal NP inks to preserve oxidation state and prevent agglomeration has unintended consequences on the print quality.

Plasma jet printer (PJP) has recently emerged as a single-step alternative to IJP and AJP, solving all of the issues mentioned above [26], [27], [28], [29], [30], [31], [32]. Plasma printing, in a nutshell, is AJP with the aid of plasma. Instead of using the carrier gas to just transport and deliver NP inks to the substrate (as in AJP), the carrier gas in the plasma printer is in the form of a cold atmospheric pressure dielectric barrier discharge (DBD). The combination of the effects from electrons, ions, active radicals, UV, and mild residual heat enables good adhesion of the material to the substrate, eliminating the need for the postannealing or curing step. As this is a newly emerging technology, we provide in this tutorial article an introduction to plasma printing, principles of operation, printer hardware, and some sample results.

II. LOW-TEMPERATURE PLASMAS

Low-temperature plasmas have long been used in IC manufacturing, featuring in critical processes, such as RIE, thin-film sputtering, and plasma-enhanced chemical vapor deposition. These are mostly low-pressure systems (operating at few millitorr pressure) at thermodynamic nonequilibrium [33]. Electron temperatures are typically 2-4 eV, ion temperatures in the range of 0.25–0.5 eV, and gas temperatures 300 K–800 K. The discharge in the above applications is sustained by capacitive or inductive power sources and the charged particle/neutral ratio is typically $<10^{-3}$. Atmospheric pressure plasmas, primarily confined to micrometer scale dimensions and thus called microplasmas [34], [35], [36], have gained popularity in the last two decades. Microplasmas feature high electron densities in small volumes, and their high surface area to volume ratio results in high power densities. They have found extensive applications in indoor air purification, sterilization, light sources, lasers, surface modification, medical treatment (skin and teeth), nanomaterial synthesis, plasma reactors, ozone generation, actuators for flow control, and others [34], [35], [36]. Nevertheless, microplasmas have not been explored for printing until recently [26], [27], [28], [29], [30], [31], [32]; only common use of any type of plasma in FPE has been for posttreatment of inkjet or AJP films, i.e., the so-called plasma sintering [37], [38], as an alternative to thermal and laser sintering [23] and also for the removal of unwanted organic and other contaminant residues from substrates and devices.

Although microplasmas vary widely [34], [35], [36] in most applications and are classified by the power sources, electrode configurations, frequency, and other key plasma parameters, the plasma in printing applications has been mainly DBD of an inert gas, such as He or Ar [26], [27], [28], [29], [30], [31], [32]. A description of the plasma printer and its operation is given in the following.

III. ATMOSPHERIC PRESSURE PLASMA JET PRINTER

Building a homemade DBD system for printing purposes is straightforward, and details and schematics can be found in [27], [28], [29], and [30]. The main system consists of a glass tube, nominally 5 mm in diameter, and two copper tapes wound over the tube 2 cm apart serve as the electrodes. One electrode is grounded and the second is connected to a high-voltage ac power supply capable of 1-20 kV at 20-60-kHz frequencies. The diameter of the exit nozzle of the tube determines the print rate and throughput, with rates decreasing with the nozzle size. The nozzle size can be as small as 10 μ m for high-resolution printing. Helium or argon can be used as carrier gas. The feed system to the plasma region consists of two inputs or inlets. One is the "dry gas," where the carrier gas alone is fed at the desired rate metered by a mass flow controller and this creates the standing DBD in the tube. The second is the "wet gas," which consists of the carrier gas plus the ink colloids or NPs generated through a nebulizer and delivered to the plasma region through a second mass flow controller. No vacuum pump is needed since the printer works at atmospheric pressure. Application of a voltage to the powered electrode initiates and sustains the DBD and the plasma exiting the nozzle strikes the substrate placed closely (2–5 mm) resulting in the printing of the desired material.

A wide range of metals (Ag, Cu, and Au), semiconductors and oxides (TiO₂, SnO₂, CuO, and ZnO), graphene, carbon nanotubes (CNTs), and dielectrics (SiO₂) has been plasma-printed using both the homemade system described above and commercial tool (described in the following) on various substrates, including paper, cotton, glass, silicon, polyimide, polyethylene terephthalate (PTFE), printed circuit board (PCB), and 3-D polymer objects [26], [28], [29], [30], [31], [32], [39]. No postthermal treatment was needed in any of the above cases, and instead, as-printed samples provided desired consolidated thin films. For example, the comparison of printed CNTs on paper with plasma on and off (latter corresponding to AJP) revealed higher nanotube density, very good interconnectivity, denser film, and conductance for the plasma-printed case with three orders of magnitude higher conductance compared to the AJP case [28]. Similar plasma on versus off control studies in silver [26] and graphene [29] printing also showed much higher conductance upon printing compared to plasma-off samples, which need a sintering step to get meaningful conductivities.

The inherent nature of cold plasmas allows good quality printing, manifesting in the following advantages over IJP and AJP. The active material ink or NPs is carried with the electrons and ions, active atoms, and radicals to the substrate in an environment that has UV and some mild heat. The NPs may get charged in the plasma as well through charge exchange

reactions. The microplasma typically looks continuous to the naked eye, but previous studies using high-speed nanosecondresolved photography showed the plasma as high-speed "bullets" [40] emerging out of the nozzle with velocity exceeding that of the gas by four orders of magnitude [40], [41]. This whole complex environment appears to result in a "selfsintering" effect providing good adhesion of the film onto the substrate upon the material strike on the substrate. In other words, the "sticking coefficient" is high compared to the scenario with the plasma off (pure aerosol only), eliminating the need for the annealing or curing step. Comprehensive studies correlating the plasma and surface conditions to the observed printing results and adhesion, measurement of sticking coefficients with the plasma on and off, and investigations into reaction kinetics are needed to gain insight, which can be facilitated by plasma diagnostics, surface diagnostics, and modeling.

The self-sintering discussed above may not always be complete within the time frame of the printing, and additional exposure of the printed sample to the inert plasma (without the ink supply) may be warranted. Understanding this needs examination of the general role of sintering itself. The sintering step, regardless of the self-sintering here or the posttreatment needed with IJP and AJP, achieves two functions. The first is the promotion of connectivity of the NPs on the substrate forming a film, effectiveness of which increases with energy input (heat, laser, plasma, etc.). This is a necessary physical effect converting delivered NPs into a film to improve the morphology, conductivity, and other properties. The second is the elimination of all unwanted constituents, such as solvent, binders, surfactants, and many other additives, all of which—if not removed—suppress the film quality through the deviation of properties from the corresponding bulk values. This aspect of printing is really undesired, even a nuisance, since most commercial inks do not reveal the identity of many of the ink constituents for proprietary reasons, which necessarily results in significant number of trial and error experiments for the user on the removal process, i.e., optimizing sintering conditions. It is clear then the quality of the ink and postprocessing to remove everything other than the target material constituent from the printed film determine the device performance and eventual success of FPE in intended applications. This discussion provides the context, where exposure of the printed sample to the inert gas plasma for a short period may be warranted in some cases upon the completion of the printing, as demonstrated before [29], [32]. From the first point of view, the NPs in the ink may not be of uniform size, and the tuned plasma conditions for printing may not complete self-sintering for those NPs exceeding the mean size. From the second point of view, the presence of excessive amount of the secondary/unwanted materials in the ink may need higher energy input over a longer period for removal. Inert plasma exposure can achieve both functions without the need for additional equipment or sample transfer. Finally, if a particular combination of ink-substrate needs pretreatment in some rare cases, again it can be achieved in the printer itself (either with some inert gas or reactive gas plasma as the case may be) without the need for additional equipment.

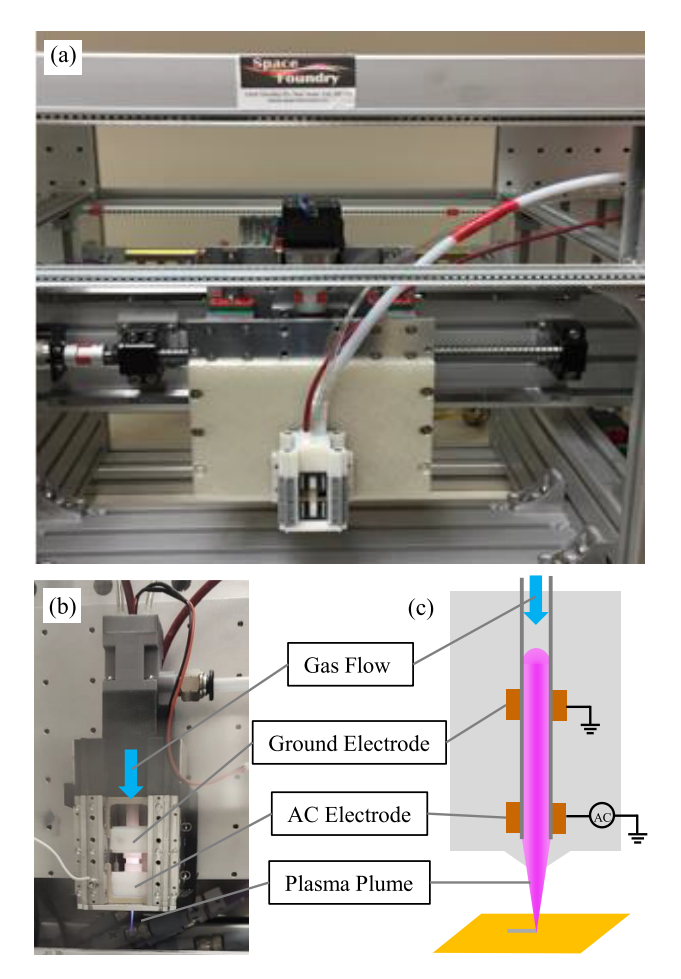


Fig. 1. (a) Plasma printer showing the print head. (b) Expanded view of the print head. (c) Schematic showing various parts.

There are a few other advantages offered by plasma printing over competing techniques. Printing of some metals can be achieved with cheaper oxide inks instead of expensive metallic inks. For example, copper printing has been demonstrated using copper oxide ink by diluting the carrier gas with less than 5% of H₂ [30]. The atomic hydrogen produced in the plasma reduces copper oxide to Cu on the fly and helps to print high-quality Cu patterns. The reducing atomic hydrogen environment has also been exploited to print graphene from inexpensive graphene oxide ink [29]. Printing of gold using HAuCl₄ solution instead of expensive nano gold ink has been shown to give excellent quality film ideally suited for surface-enhanced Raman spectroscopy applications [31], [32]. Finally, the plasma characteristics can be exploited to tailor the properties of the material passing through it in situ, for example, oxidation state, dielectric constant, electronic conductivity, and others [30].

Fig. 1 shows a commercial plasma printer (Space Foundry, San Jose, CA, USA) that incorporates all of the above features. The print head, the heart of the system, is shown inside the printer enclosure as in most common printers [39]. The print head can also be mounted on a robotic arm as seen in Fig. 2 to enable printing on arbitrarily shaped objects and over large areas, suited for manufacturing. The print head includes all the features of the homemade system discussed earlier in a compact fashion with a 0.8-mm-diameter dielectric tube and

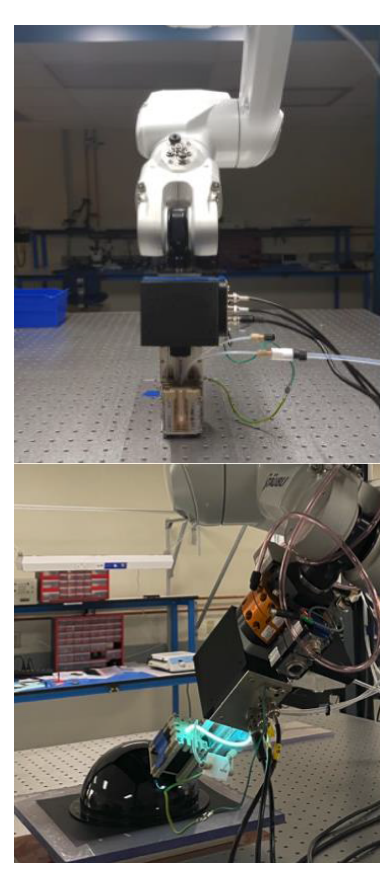


Fig. 2. Print head mounted on a robotic arm (top) and printing on a dome (bottom).

1.5-cm electrode gap. Two mass flow controllers supply the wet gas and dry gas into the print head, and the atomizer can generate 3–8- μ m size droplets. The print resolution is essentially dependent on the nozzle diameter and print head dimensions. The plasma jet technology does not pose a limitation on high resolution as the fluid flow in the nozzle is controlled by electromagnetic field and plasma. Nevertheless, there could be fundamental limits to the resolution and technology since continued reduction in nozzle size and print head dimensions would result in changes of the forced required to keep the flow continuing. These considerations may also have an impact on the materials used and overall design and these need careful evaluation in the future. The current in PJP is only at the milliampere level by placing a dielectric between the electrodes unlike in the high-temperature arc jet technology used in welding and metallurgical applications featuring several amps of current. The inert gas plasma in general is stable under the printing conditions and stable plasma is prerequisite for printing. Further peripheral details on the printer including various safety and control features can be found in [39].

The "knobs" available to control print characteristics include applied voltage on the powered electrode and wet and dry gas flow rates. Besides, the loading fraction of the ink, concentration of the ink, and aerosol characteristics, such as droplet size, can be adjusted as well. Finally, the inert gas exposure time upon the completion of the printing, if needed, can be varied to control the morphology and obtain the best conductivity

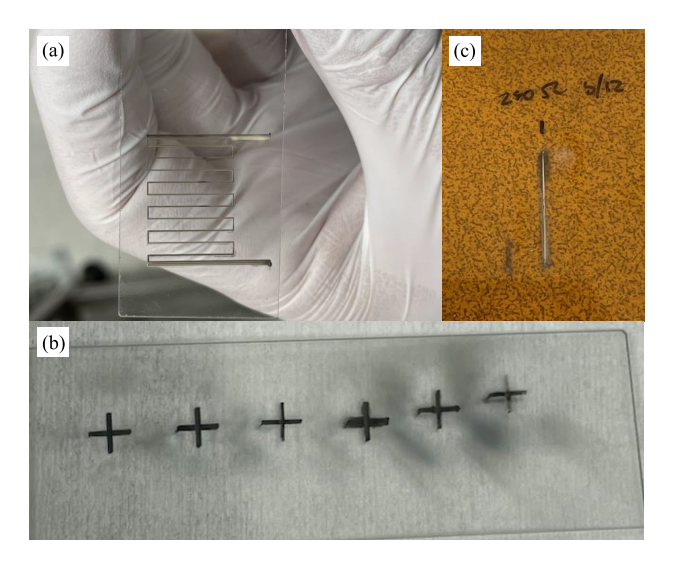


Fig. 3. Plasma printed silver patterns on (a) and (b) glass and (c) polyimide.

and other relevant properties. Some sample results from this printer are presented in the following.

IV. PRINTING RESULTS

Fig. 3 shows the representative plasma-printed silver patterns. Ag was printed on rigid and flexible substrates, including glass, polyimide, and paper. The serpentine Ag pattern shown in Fig. 3 was printed on glass using helium plasma at 15 kV and a resonant frequency of 27.6 kHz. A commercial ink (Novacentrix Metalon JS-A221AE) was used with 150 and 350 sccm of wet and dry gas flow rates, respectively. A single layer was printed with the nozzle 2 mm from the substrate with a print speed of 0.1 mm/s. The gas flow rates, print height, and speed have a direct correlation to the quality and characteristics of the printed film. For example, the silver four-point structures in Fig. 3(b) were printed on glass with varying dry gas flows, and the linewidth and overspray changed dramatically with the change in helium flow parameters. Thicknesses of the printed lines were measured with stylus profilometry (Bruker DektakXT). The average step height was extracted over the width of the printed line, so that the area could be calculated. Three measurements were taken at different points of each printed line to get an average of the profile. The three measurements were averaged and multiplied with the width to calculate the average area (cross-sectional) of each line. This area was then used to calculate the conductivity of the printed lines. The resistance of the as-printed 20×0.43 mm line with 14 μ m thickness in Fig. 3(c) is 250 Ω end to end, and the resulting conductivity is a very small fraction of the bulk silver conductivity. Increasing the plasma voltage steadily increases the conductivity as seen in Fig. 4.

Fig. 4 shows silver lines printed at various plasma voltages and the conductivity of as-printed sample increases with the plasma voltage [see Fig. 4(c)]. An increase in sintering is observed as NPs are exposed to more energetic plasma. Fig. 4(b) and (d) shows a cross-sectional scanning electron microscopy (SEM) image and the line profile of the same sample with good match. The SEM image shows the NPs distributed over the printed line, and the Ag NPs are self-sintered

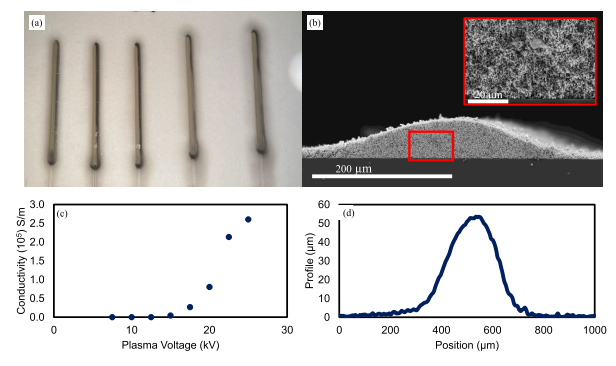


Fig. 4. (a) Plasma printed Ag lines on glass substrate as in Fig. 3(c) but at various plasma voltages. (b) Cross-sectional SEM image of a sample printed at 20 kV. (c) Increasing conductivity of as-printed sample with plasma voltage. (d) Profile of printed line of sample shown in (b) measured with a stylus profilometer.

as evident from the grain growth. The 30–50-nm particles grow and form a conductive network and the SEM reveals many particles that have grown over to 900 nm.

Gold NP ink with NPs sized under 60 nm (InFlex Labs, Boise, ID, USA) was also plasma printed on glass, polyimide, and paper substrates. Fig. 5(a) shows a printed strain gauge structure on a glossy paper substrate that would be useful for structural monitoring applications. The printer resolution was optimized to 150 μ m and the conductive pattern was printed using serpentine fill. The dry and wet gas flow rates were 350 and 100 sccm, respectively, and the helium plasma was tuned to 20 kV and 28 kHz. Fig. 5(c) shows a SEM cross section image of a Au sample printed on standard printer paper. The image shows that the plasma printer coats the NPs onto the uneven, fibrous surface just with two passes. Au was also printed on glass with varying plasma powers from 10 to 25 kV. Among ten printed samples, the peak conductivity of as-printed sample (not shown here) occurring at 12.5 kV was 8.5×10^5 S/m with no post sintering, which is $48 \times$ smaller than bulk gold conductivity. The average conductivity of the ten samples was 3.3×10^5 S/m (which is 126 times smaller than bulk conductivity), with a standard deviation of $2.7 \times$ 10⁵ S/m. This highlights the ability of the PJP to consistently produce conductive traces within an order of magnitude while acknowledging its some variability in printing. This variability can be partly addressed by tuning plasma voltage, gas flow, and ink composition for more consistent printing. In contrast to the above outcome, as-printed gold patterns using IJP feature extremely high resistance not useful for any device but improve only upon sintering, for example, to 5×10^6 S/m when subjected to sintering of 250 °C for 1 h or 200 °C for 6 h [42] and in another study, to 2.5×10^6 S/m when sintered at 155 °C and 7.6 \times 10⁶ S/m at 200 °C both lasting 75 min [22]. Finally, the as-printed films of all materials on various substrates generally show good adhesion based on the scotch tape test.

Bismuth telluride (Bi₂Te₃) has excellent thermoelectric properties at room temperature and is being studied for use in low-temperature thermoelectric generators [43]. Colloidal ink containing Bi₂Te₃ nanoflakes was printed using the plasma printer on polyimide to create legs for flexible thermoelectric generators. Fig. 6(a) shows an array of thermoelectric legs

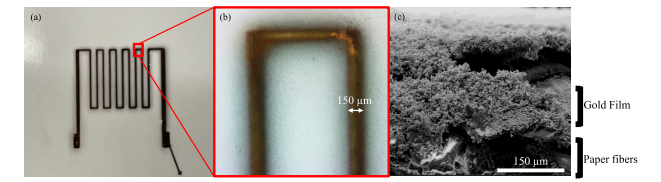


Fig. 5. Plasma printed gold patterns on paper. (a) Strain gauge structure. (b) Expanded view of (a). (c) SEM image.

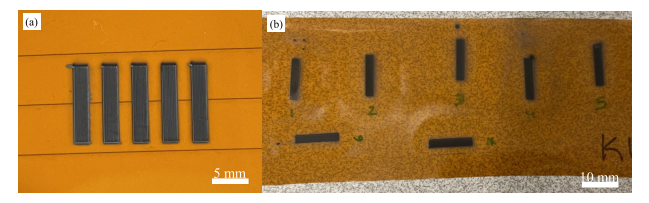


Fig. 6. Bi₂Te₃ thermoelectric legs plasma printed on polyimide. (a) multi-leg device and (b) single legs.

printed on polyimide with 350 and 100 sccm dry and wet gas flow, respectively. The plasma conditions were 15 kV and 27.6 kHz, with the nozzle about 2 mm from the substrate. The 2 \times 10 mm legs were filled using three passes of 50- μ m serpentine pattern with a printed line thickness of about 150- μ m lines to increase overlap and overall film thickness. Fig. 6(b) shows 2 \times 12 mm legs printed on polyimide during optimization of the ink. The characterization of electrical and thermoelectric properties of these legs can be found in [44]. Fig. 6 shows the capability of the plasma printer to print versatile materials beyond just metals.

V. CONCLUSION

This tutorial introduced a new application of microplasmas in 2-D printing and discussed the principles and operation of PJP. The unique advantages include the ability to obtain consolidated thin films upon printing without any thermal treatment, plasma chemistry allowing the use of versatile precursors, reducing environment enabled by hydrogen dilution of the carrier gas to print metals and other elements from their respective (cheaper) oxide inks, and finally, the ability to alter properties in situ by tuning the plasma conditions. The demonstrated printing results to date appear promising and provide evidence to the potential of plasma printing in printed and flexible electronics. Also, recent demonstration of plasma printing of metallic patterns in zero gravity attests to the robustness of the printing technique and hardware [45]. The technology nevertheless is new and further work is warranted in several areas for a wide range of commercial applications, for example, feature resolution under 50 μ m, establishing the effect of process variables on printing, effectiveness of inert plasma treatment (and the time needed) as an alternative to external sintering step, and generation of data on key metrics, such as printing throughput, long duration printing, overspray, line edge roughness, and so on. Plasma diagnostics, aided by plasma modeling, would provide valuable information on electron and ion densities, electron and ion temperatures, plasma electric filed, and so on that can be correlated with print quality to enable tuning of the available knobs and obtain desired printing performance. A systematic comparison of performance with other established printing techniques is needed for the printing of various materials.

ACKNOWLEDGMENT

The authors would like to thank Pranay Doshi, Daniel Gutierrez, and Dennis Nordlund (Space Foundry Inc.) for their contributions and Curtis Hill (NASA Marshall Space Flight Center) and Jessica Koehne (NASA Ames Research Center) for their support of technology development.

REFERENCES

- [1] L. Yang, R. Zhang, D. Staiculescu, C. P. Wong, and M. M. Tentzeris, "A novel conformal RFID-enabled module utilizing inkjet-printed antennas and carbon nanotubes for gas-detection applications," *IEEE Antennas Wireless Propag. Lett.*, vol. 8, pp. 653–656, 2009.
- [2] E. Singh, M. Meyyappan, and H. S. Nalwa, "Flexible graphene-based wearable gas and chemical sensors," ACS Appl. Mater. Interfaces, vol. 9, no. 40, pp. 34544–34586, Sep. 2017.
- [3] S. Guler, B. Karaosmanoglu, and O. Ergul, "Design, simulation, and fabrication of a novel type of inkjet-printed pixel antennas," *Prog. Electromagn. Res. Lett.*, vol. 64, pp. 51–55, 2016.
- [4] S. Amendola, A. Palombi, and G. Marrocco, "Inkjet printing of epidermal RFID antennas by self-sintering conductive ink," *IEEE Trans. Microw. Theory Techn.*, vol. 66, no. 3, pp. 1561–1569, Mar. 2018.
- [5] A. M. Gaikwad, A. C. Arias, and D. A. Steingart, "Recent progress on printed flexible batteries: Mechanical challenges, printing technologies, and future prospects," *Energy Technol.*, vol. 3, no. 4, pp. 305–328, Apr. 2015.
- [6] M. L. Seol et al., "All-printed in-plane supercapacitors by sequential additive manufacturing process," ACS Appl. Energy Mater., vol. 3, no. 5, pp. 4965–4973, 2020.
- [7] H. Zhang, Y. Qiao, and Z. Lu, "Fully printed ultraflexible supercapacitor supported by a single-textile substrate," ACS Appl. Mater. Interfaces, vol. 8, no. 47, pp. 32317–32323, Nov. 2016.
- [8] S. Jang, S. Kim, M. L. Geier, M. C. Hersam, and A. Dodabalapur, "Inkjet printed carbon nanotubes in short channel field effect transistors: Influence of nanotube distortion and gate insulator interface modification," *Flexible Printed Electron.*, vol. 1, no. 3, Sep. 2016, Art. no. 035001.
- [9] B. Huber, P. B. Popp, M. Kaiser, A. Ruediger, and C. Schindler, "Fully inkjet printed flexible resistive memory," *Appl. Phys. Lett.*, vol. 110, no. 14, Apr. 2017, Art. no. 143503.
- [10] K. J. Yoon et al., "Electrically-generated memristor based on inkjet printed silver nanoparticles," *Nanoscale Adv.*, vol. 1, no. 8, pp. 2990–2998, 2019.
- [11] K. Rajan, E. Garofalo, and A. Chiolerio, "Wearable intrinsically soft, stretchable, flexible devices for memories and computing," *Sensors*, vol. 18, no. 2, p. 367, Jan. 2018.
- [12] M. L. Seol, J. W. Han, D. I. Moon, K. J. Yoon, C. S. Hwang, and M. Meyyappan, "All-printed triboelectric nanogenerator," *Nano Energy*, vol. 44, pp. 82–88, Feb. 2018.
- [13] M. Cuartero, M. Parrilla, and G. Crespo, "Wearable potentiometric sensors for medical applications," *Sensors*, vol. 19, no. 2, p. 363, Jan. 2019.
- [14] D. I. Moon et al., "On-demand printing of wearable thermotherapy pad," Adv. Healthcare Mater., vol. 9, no. 4, 2020, Art. no. 1901575.
- [15] K. Yan, J. Li, L. Pan, and Y. Shi, "Inkjet printing for flexible and wearable electronics," APL Mater., vol. 8, no. 12, Dec. 2020, Art. no. 120705.
- [16] M. Singh, H. M. Haverinen, P. Dhagat, and G. E. Jabbour, "Inkjet printing—Process and its applications," *Adv. Mater.*, vol. 22, no. 6, pp. 673–685, Feb. 2010.
- [17] V. Beedasy and P. J. Smith, "Printed electronics as prepared by inkjet printing," *Materials*, vol. 13, no. 3, p. 704, Feb. 2020.
- [18] G. Cummins and M. P. Y. Desmulliez, "Inkjet printing of conductive materials: A review," *Circuit World*, vol. 38, no. 4, pp. 193–213, 2012.
- [19] J. M. Hoey, A. Lutfurakhmanov, D. L. Schulz, and I. S. Akhatov, "A review on aerosol-based direct-write and its applications for microelectronics," *J. Nanotechnol.*, vol. 2012, Sep. 2012, Art. no. 324380, doi: 10.1155/2012/324380.
- [20] Heterogeneous Integration Roadmap, 2021 Edition, Chapter 22: Interconnects for 2D and 3D architectures; Chapter 23: Wafer Level Packaging; IEEE. Accessed: Jul. 18, 2022. [Online]. Available: https://eps.ieee.org/technology/heterogeneous-integration-roadmap/2021-edition.html Last
- [21] B. Khorramdel, T. M. Kraft, and M. Mantysalo, "Inkjet printed metallic micropillars for bare die flip-chip bonding," *Flexible Printed Electron.*, vol. 2, no. 4, 2017, Art. no. 045005.

- [22] J. A. Sadie and V. Subramanian, "Three-dimensional inkjet-printed interconnects using functional metallic nanoparticle inks," *Adv. Funct. Mater.*, vol. 24, no. 43, pp. 6834–6842, Nov. 2014.
- [23] A. Roshanghias, M. Krivec, and M. Baumgart, "Sintering strategies for inkjet printed metallic traces in 3D printed electronics," *Flexible Printed Electron.*, vol. 2, no. 4, Dec. 2017, Art. no. 045002.
- [24] W. Li et al., "The rise of conductive copper inks: Challenges and perspectives," Appl. Mater. Today, vol. 18, Mar. 2020, Art. no. 100451.
- [25] D. Grbovic, F. D. Alves, R. Mattish, D. Lee, J. W. Han, and M. Meyyappan, "Rapid prototyping of microwave metasurfaces by ink-jet printing on polyester (PET) transparencies," *Flexible Printed Electron.*, vol. 5, no. 4, 2020, Art. no. 045003.
- [26] R. P. Gandhiraman, V. Jayan, J.-W. Han, B. Chen, J. E. Koehne, and M. Meyyappan, "Plasma jet printing of electronic materials on flexible and nonconformal objects," ACS Appl. Mater. Interfaces, vol. 6, no. 23, pp. 20860–20867, Dec. 2014.
- [27] R. P. Gandhiraman, D. Nordlund, V. Jayan, M. Meyyappan, and J. E. Koehne, "Scalable low-cost fabrication of disposable paper sensors for DNA detection," ACS Appl. Mater. Interfaces, vol. 6, no. 24, pp. 22751–22760, Dec. 2014.
- [28] R. P. Gandhiraman, E. Singh, D. C. Diaz-Cartagena, D. Nordlund, J. Koehne, and M. Meyyappan, "Plasma jet printing for flexible substrates," Appl. Phys. Lett., vol. 108, no. 12, Mar. 2016, Art. no. 123103.
- [29] A. Dey, S. Krishnamurthy, J. Bowen, D. Nordlund, M. Meyyappan, and R. P. Gandhiraman, "Plasma jet printing and in situ reduction of highly acidic graphene oxide," ACS Nano, vol. 12, no. 6, pp. 5473–5481, Jun. 2018.
- [30] A. Dey et al., "Plasma jet based in situ reduction of copper oxide in direct write printing," J. Vac. Sci. Technol. B, Microelectron., vol. 37, no. 3, 2019, Art. no. 031203.
- [31] J. Hong et al., "Direct plasma printing of nano-gold from an inorganic precursor," J. Mater. Chem. C, vol. 7, no. 21, pp. 6369–6374, 2019.
- [32] R. Alder et al., "Application of plasma-printed paper-based SERS substrate for cocaine detection," Sensors, vol. 21, no. 3, p. 810, 2021.
- [33] M. A. Lieberman and A. J. Lichtenberg, *Principles of Plasma Discharges and Materials Processing*, 2nd ed. Hoboken, NJ, USA: Wiley, 2005.
- [34] W. Chiang, D. Mariotti, R. M. Sankaran, J. G. Eden, and K. Ostrikov, "Microplasmas for advanced materials and devices," *Adv. Mater.*, vol. 32, no. 18, May 2020, Art. no. 1905508.
- [35] K. H. Becker, "25 years of microplasma science and applications: A status report," *Plasma Phys. Technol.*, vol. 5, no. 1, pp. 5–9, 2018.
- [36] R. Brandenburg, "Dielectric barrier discharges: Progress on plasma sources and on the understanding of regimes and single filaments," *Plasma Sources Sci. Technol.*, vol. 26, no. 5, Mar. 2017, Art. no. 053001.
- [37] N. Turan, M. Saeidi-Javash, J. Chen, M. Zeng, Y. Zhang, and D. B. Go, "Atmospheric pressure and ambient temperature plasma jet sintering of aerosol jet printed silver nanoparticles," ACS Appl. Mater. Interfaces, vol. 13, no. 39, pp. 47244–47251, Oct. 2021.
- [38] C. Wang, I. C. Cheng, and J. Z. Chen, "Ultrafast atmospheric-pressureplasma-jet sintering of nanoporous TiO₂-SnO₂ composites with features defined by screen-printing," ECS J. Solid State Sci. Technol., vol. 4, no. 4, pp. P3020–P3025, 2015.
- [39] R. Ramamurti et al., "Atmospheric pressure plasma printing of nanomaterials for IoT applications," *IEEE Open J. Nanotechnol.*, vol. 1, pp. 47–56, 2020.
- [40] M. Teschke, J. Kedzierski, E. G. Finantu-Dinu, D. Korzec, and J. Engemann, "High-speed photographs of a dielectric barrier atmospheric pressure plasma jet," *IEEE Trans. Plasma Sci.*, vol. 33, no. 2, pp. 310–311, Apr. 2005.
- [41] X. Lu and M. Laroussi, "Dynamics of an atmospheric pressure plasma plume generated by submicrosecond voltage pulses," *J. Appl. Phys.*, vol. 100, no. 6, Sep. 2006, Art. no. 063302.
- [42] Y. Khan et al., "Inkjet-printed flexible gold electrode arrays for bioelectronic interfaces," Adv. Funct. Mater., vol. 26, no. 7, pp. 1004–1013, 2016
- [43] C. Hollar et al., "High-performance flexible bismuth telluride thin film from solution processed colloidal nanoplates," Adv. Mater. Technol., vol. 5, no. 11, 2020, Art. no. 2000600.
- [44] J. Manzi et al., "Plasma-jet printing of colloidal thermoelectric Bi Te nanoflakes for flexible energy harvesting," *Nanoscale*, 2023, doi: 10.1039/d2nr06454e.
- [45] D. H. Gutierrez, P. Doshi, D. Nordlund, and R. P. Gandhiraman, "Plasma jet printing of metallic patterns in zero gravity," Flexible Printed Electron., vol. 7, no. 2, Jun. 2022, Art. no. 025016.